Supporting Information

A high-performance crystalline $Ti_2O_{1.3}(PO_4)_{1.6}/TiO_2$ carbon-coated composite as an anode for lithium-ion batteries

Yayun Zheng,[a,b] Yuefo Yi,[a] Ziyi Yang,[a,c] Wenbin Zhou,[b] Yichao Wang[d] and Zhengfei Chen*[a]

[a]School of Biological and Chemical Engineering, NingboTech University, Ningbo, Zhejiang 315100, P. R. China.

[b]Zhejiang Oceanking Development Co., Ltd., Ningbo, Zhejiang 315204, P. R. China.

[c]College of Chemical Engineering, Zhejiang University of Technology, Hangzhou, Zhejiang 310014, P. R. China.

[d]School of Engineering, Design and Built Environment, Western Sydney University, Penrith, NSW 2751, Australia.

*Corresponding author: Zhengfei Chen
E-mail: E-mail: zhengfei.chen@nit.zju.edu.cn

Experimental

All chemicals (grade A.R.) were purchased directly from chemical companies. Titanium isopropoxide (TIP, Macklin, 95%), 1-butyl-3-methylimidazolium bromide ([Bmim]Br, Aladdin Biochemical, 98%), KPF_6 (Merck, 99%), acetonitrile (Aladdin Biochemical, 99%), glucose (Aladdin Biochemical, 99%), polyvinylidene fluoride (PVDF, Kynar HSV900, Arkema), Acetylene black (AB, Wako Pure Chemical Industries, purity > 99.99%), and N-methyl pyrrolidone (NMP, Tianjin Damao) was used as purchased.

In this work, $[Bmim]PF_6$ were firstly synthesized according to the procedure described in our previous work.[1] In a typical synthesis, [Bmim]Br (21.9 g, 100 mmol) and KPF_6 (18.6 g, 101 mmol) were introduced into 50 mL of acetonitrile, followed by heating at 70 °C for a period of 2 days. Upon completion, the solution underwent filtration to eliminate the KBr salt. Subsequently, the filtrate was further evaporated using a rotary evaporator to obtain a white liquid of $[Bmim]PF_6$.

For the preparation of C@TOP/TO, an improved $[Bmim]PF_6$-assisted hydrothermal method using glucose modification was applied in this study.[1] Firstly, 1.5 g of TIP and 1 g of $[Bmim]PF_6$ were mixed under stirring. Then, 1 mL of H_2O was gradually added, resulting in the immediate formation of a white precipitate. After stirring for 2 min, 11 g of H_2O and 0.3 g of glucose were added. The mixture was stirred at room temperature for 1 hour, then transferred to a 50 mL Teflon-lined autoclave and reacted at 150 °C for 12 h in a conventional oven. Following this, the reaction material was dried in a 70 °C oven for 12 h without cleaning. The calcination was then performed on the dried material in a tube furnace with a rate of 3 °C/min under N_2. After a two-hour hold at 450 °C, the final sample C@TOP/TO-0.3 was obtained. For comparison, the $[Bmim]PF_6$-assisted hydrothermal method without glucose modification (0 g of glucose) was employed, followed by the same calcination procedure to obtain C@TOP/TO-0. The same calcination procedure was also carried out solely on glucose to obtain GD-C.

To examine the crystal phase of C@TOP/TO-0, C@TOP/TO-0.3, and GD-C samples, X-ray diffraction (XRD) analysis was conducted using a Philips diffractometer with Cu *K*α radiation (λ = 0.15406 nm). X-ray photoelectron spectroscopy (XPS) was performed on a Thermo Scientific spectrometer (Al *K*α radiation) to analyze the surface chemistry of C@TOP/TO-0.3. Scanning electron microscopy (SEM) images of the three samples were captured using a field-emission scanning microscope (Hitachi Regulus8230) to

compare their morphology, which was coupled with an energy dispersion X-ray spectroscopic (EDX) mapping (Horiba EMAXEvolution) to analyze the elemental distribution over the C@TOP/TO-0.3. To obtain the structural morphology, a JEOL JEM-F200 transmission electron microscope was utilized for the Transmission electron microscopy (TEM) examination of the C@TOP/TO-0.3 sample. To evaluate the Brunauer–Emmett–Teller (BET) surface area and Barrett−Joyner−Halenda (BJH) pore size of these three samples, N_2 adsorption-desorption isotherms were conducted using a Micromeritics 3000 Tristar surface area and porosity analyzer at 77 K. Prior to the analysis, the samples were vacuum degassed at 120 °C for at least 5 hours. Thermogravimetry (TG) measurement was carried out in air from 30 to 900 °C at a heating speed of 20 °C min^{-1} on Netzsch TG209F1 thermal gravimetric analyzer in order to analyze the carbon content of the three samples.

The synthesized samples (80 wt%) were mixed with AB (10 wt%) and PVDF (10 wt%) in NMP solvent to form a uniform slurry, where PVDF is used as the binder due to its advantageous properties in terms of chemical corrosion resistance, electrochemical stability and adhesion between active materials, conductive agents, and current collectors.[2] The slurry was subsequently coated onto a Cu foil and dried under vacuum at 90 °C for 5 hours. Finally, the dried coating was cut into disks with a diameter of 12 mm to obtain the working electrodes with a loading mass of ∼1 mg. In the Ar-filled glovebox, coin cells (2032-type) were assembled using the working electrodes and a Li metal (Wuxi Sun energy Lithium Industrial Co., Ltd.) counter electrode fixed on a stainless steel (SUS316L) plate current collector. The electrolyte used was battery-grade 1 M $LiPF_6$/EC:DMC (1:1 in volume, Shenzhen Kejing Co. Ltd.; EC: ethylene carbonate; DMC: dimethyl carbonate). Prior to cell assembling, the Celgard 2400 polypropylene film was immersed in the electrolyte and served as the separator. For all cells, the applied current and resulting capacity were calculated based on the weight of active material (∼1 mg) for C@TOP/TO-0, C@TOP/TO-0.3, and GD-C using the following equation:

Capacity (mA h g^{-1}) = Current (mA) x Time (h) / Mass of the active material (g)

The galvanostatic charge-discharge measurements were carried out using a Neware

BTS-4000 battery test instrument (Shenzhen Neware Electronics, China) at constant current rates ranging from 20 to 1000 mA g^{-1} in the voltage range of 0.05−3.0 V (versus Li^+/Li). The electrochemical impedance spectroscopy (EIS) was performed using a compact potentiostat (CompactStat e10800, Ivium) with a perturbation amplitude of 10 mV over a frequency range of 10−100 kHz. For all charge-discharge tests, the capacity retention % was calculated based on the specific discharge capacity of initial and final cycles using the following equation:

Capacity retention % = (Final capacity value / Initial capacity value) x 100

The Coulombic efficiency % was calculated based on the specific discharge capacity and specific charge capacity within one cycle using the following equation:

Coulombic efficiency % = (Discharge capacity value / Charge capacity value) x 100

Table S1 EIS fitting parameters for Nyquist plots of C@TOP/TO-0, C@TOP/TO-0.3, and GD-C anodes shown in Fig. S11.

Sample	Resistance / Ω		
	R_{bulk}	R_{SEI}	R_{ct}
C@TOP/TO-0	1.9	23	27
C@TOP/TO-0.3	3.4	12.4	2.5
GD-C	4.9	52.8	49.6

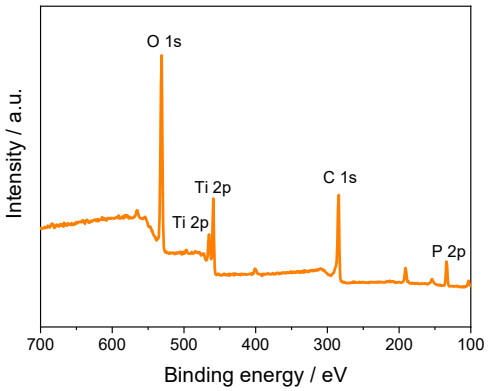

Fig. S1. The survey spectrum of C@TOP/TO-0.3 sample.

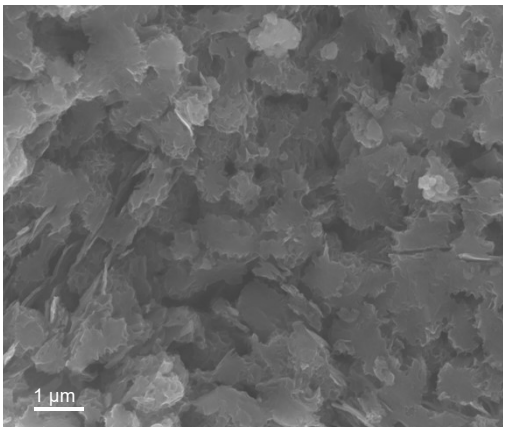

Fig. S2. SEM image of C@TOP/TO-0 sample.

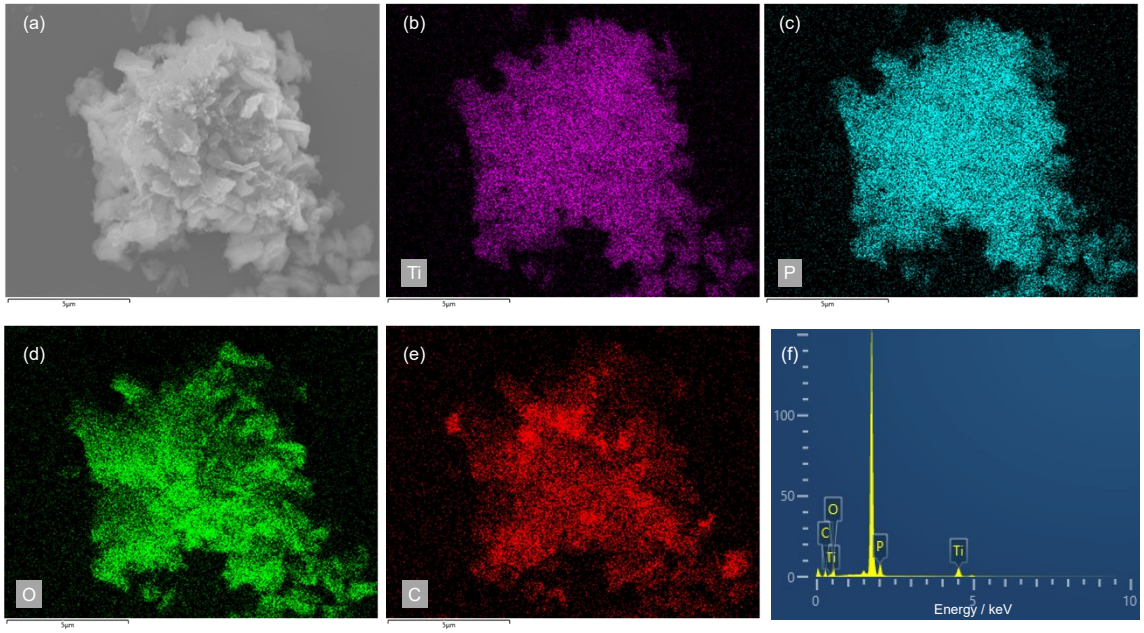

Fig. S3. (a) Low-magnification SEM image of C@TOP/TO-0.3. The corresponding EDS elemental mapping images of (b) Ti, (c) P, (d) O, (e) C, and (f) area EDS spectrum.

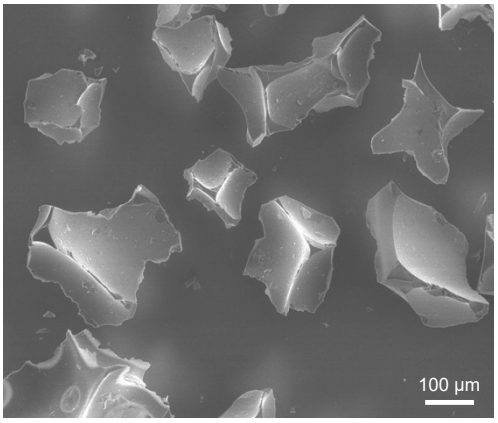

Fig. S4. SEM image of GD-C sample.

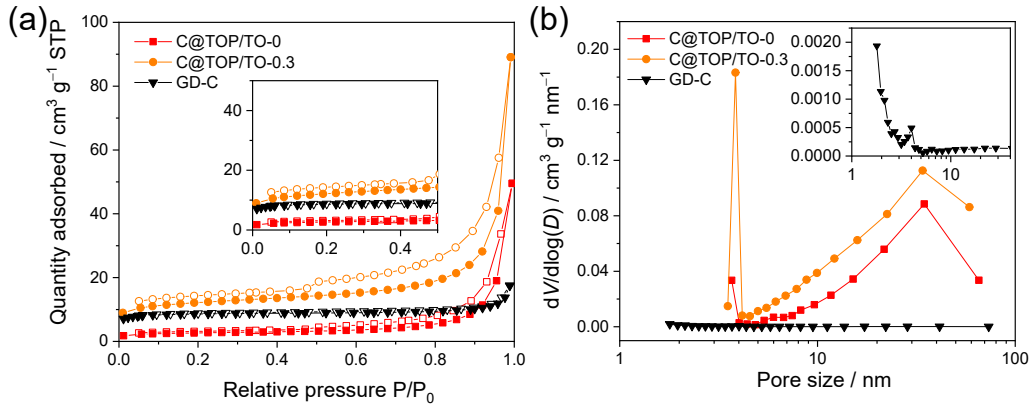

Fig. S5. (a) The N_2 adsorption-desorption isotherms of C@TOP/TO-0, C@TOP/TO-0.3, and GD-C. (b) The corresponding pore size distribution calculated by the BJH model.

Additional discussion:

As shown in Fig. S5a, the N_2 adsorption–desorption isotherms reveal that absorption saturation occurs at low relative pressure for GD-C and at high relative pressure for C@TOP/TO samples. This indicates that GD-C predominantly comprises micropores, while the C@TOP/TO samples primarily consist of mesopores.[3] This observation aligns with the findings from the pore size distribution curves (Fig. S5b). In particular, the GD-C, benefiting from its microporous structure, exhibits a large specific surface area of 26.4 m^2 g^{-1} and a higher pore volume of 0.011 cm^3 g^{-1}. Conversely, the C@TOP/TO-0 sample with thin nanosheets is inevitably stacked, resulting in a small surface area of 3.17 m^2 g^{-1} and a pore volume of 0.002 cm^3 g^{-1}, respectively. In contrast, the C@TOP/TO-0.3 nanoplates demonstrate a larger specific surface area of 9.48 m^2 g^{-1} alongside a higher pore volume of 0.011 cm^3 g^{-1} due to the significant contribution of the microporous carbon shell composed of GD-C.

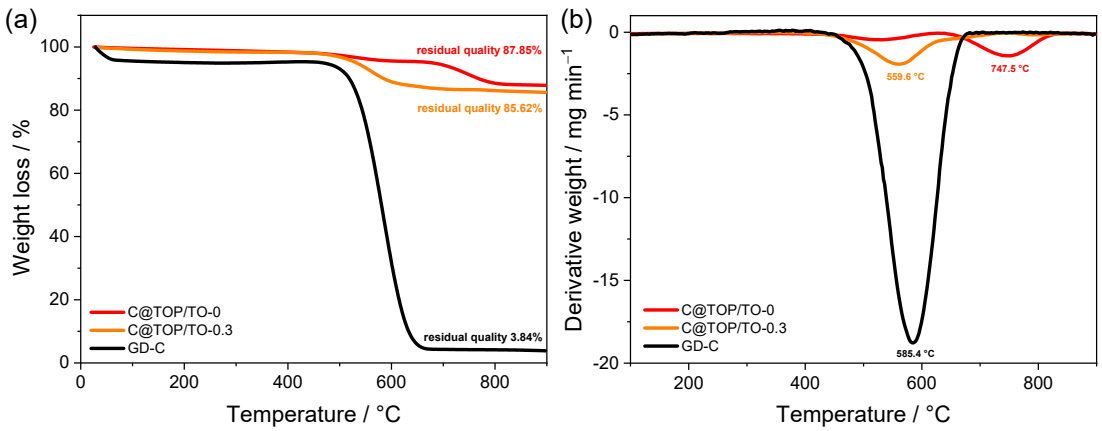

Fig. S6. (a) TG diagrams of C@TOP/TO-0, C@TOP/TO-0.3, and GD-C. (b) The corresponding DTG diagrams.

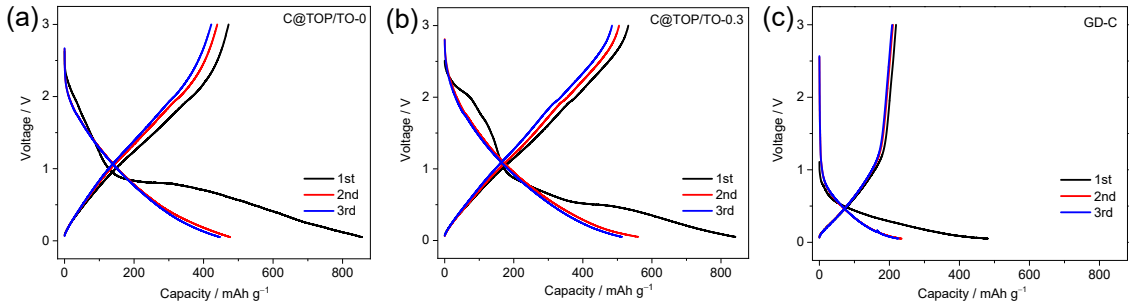

Fig. S7. The charge-discharge curves of (a) C@TOP/TO-0, (b) C@TOP/TO-0.3, and (c) GD-C anodes for the first three cycles at 20 mA g^{-1}.

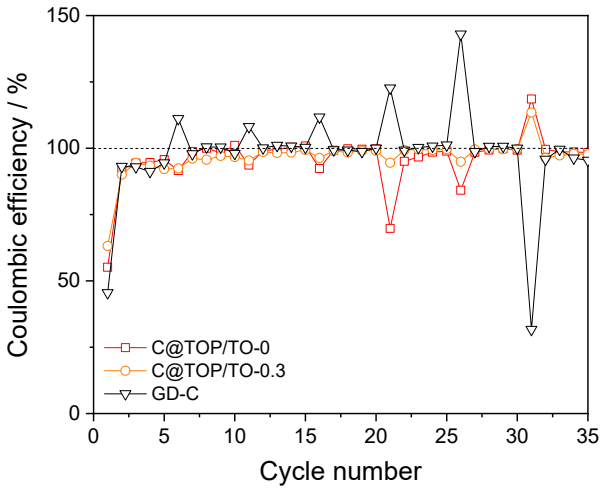

Fig. S8. The Coulombic efficiencies of C@TOP/TO-0, C@TOP/TO-0.3, and GD-C anodes in the rate test (Fig. 3a).

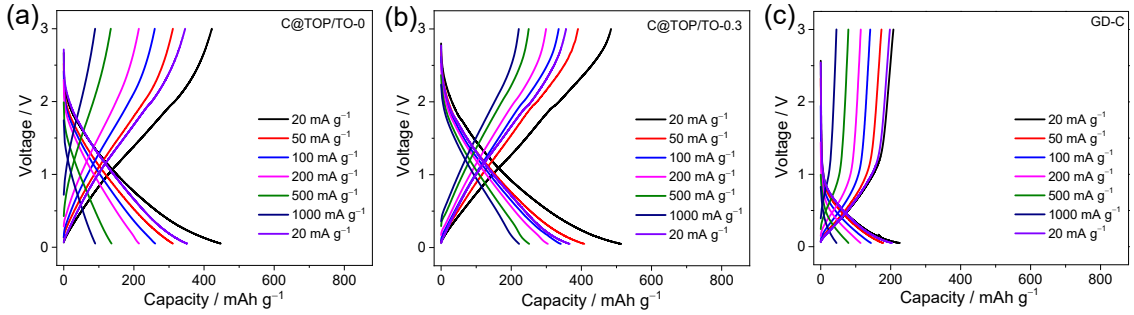

Fig. S9. The charge-discharge curves of (a) C@TOP/TO-0, (b) C@TOP/TO-0.3, and (c) GD-C anodes at different rates of 20, 50, 100, 200, 500, 1000, and 20 mA g^{-1}.

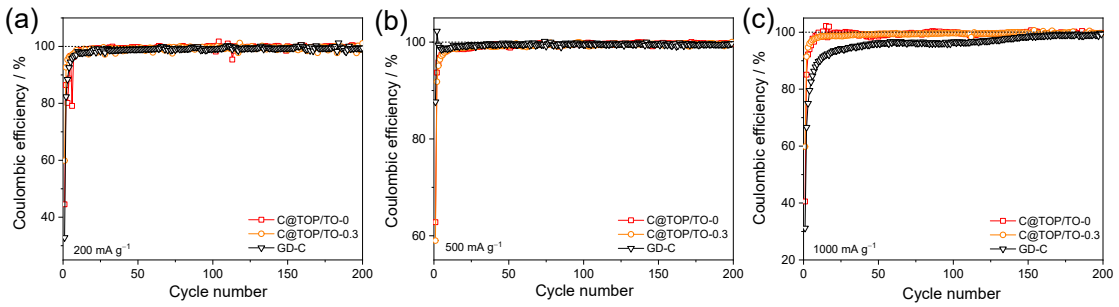

Fig. S10. The Coulombic efficiencies of C@TOP/TO-0, C@TOP/TO-0.3, and GD-C anodes in the cycle test at (a) 200 mA g^{-1}, (b) 500 mA g^{-1}, and (c) 1000 mA g^{-1} (Fig. 3b-d).

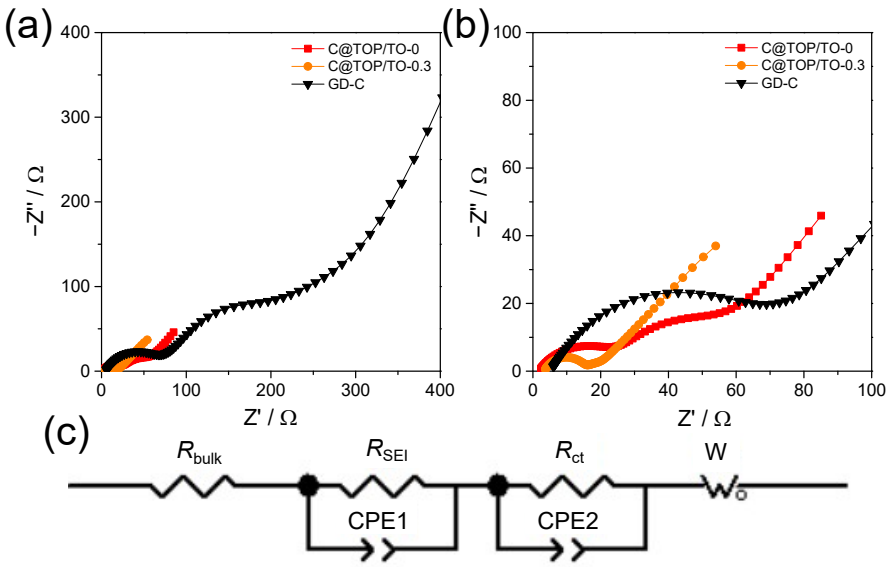

Fig. S11. Nyquist plots of C@TOP/TO-0, C@TOP/TO-0.3, and GD-C anodes.

Additional discussion:

Fig. S11 illustrates the Nyquist plots of C@TOP/TO-0, C@TOP/TO-0.3, and GD-C. These plots (Fig. S11a and b) comprising two semicircles at high frequencies and a straight line at low frequencies are fitted into the equivalent circuit shown in Fig. S11c. R_{bulk} denotes the total resistance of the electrolyte, separator, and electrode, and its value corresponds to the high-frequency intercept at the *x*-axis. R_{SEI} and R_{ct} represent the corresponding respective resistance of two semicircles in the high and low frequency ranges, corresponding to the interfacial resistance within the solid-electrolyte interface layer (SEI) and the charge transfer resistance between the electrode and the conductive agent, respectively.[4] The Warburg line is related to the diffusion of Li-ions in the bulk electrode material. See Table S1 in Supporting Information for the fitting parameters of the impedance spectra. In contrast, C@TOP/TO-0.3 exhibits the lowest R_{SEI} and R_{ct} values compared to C@TOP/TO-0 and GD-C, attesting to ameliorated ion diffusion and rapid electrochemical reaction kinetics.

References

1. R. Gao, M. Yu, H. Xu, L. Li, M. Deng, Y. Wu and Z. Chen, *Energy Fuels*, 2021, **35**, 15213−15222.
2. Z. Wu, X. Wang, S. H. K. Annamareddy, S. Gao, Q. Xu, H. Algadi, D. Sridhar, P. Wasnik, B. B. Xu, L. Weng and Z. Guo, *ES Mater. Manuf.*, 2023, **22**, 847.
3. C.-N. Feng, H.-B. Tang, X.-F. Guo, X.-L. Zhang, X.-C. Zheng and G.-P. Zheng, *Mater. Chem. Phys.*, 2020, **245**, 122785.
4. J. Zhang, G. Ji, R. Zhao, D. Li, J. Zhang, J. Liu, C. Wang, B. Zhang and X. Ou, *Appl. Surf. Sci.*, 2020, **513**, 145854.